



ELSEVIER

Nuclear Physics A 636 (1998) 209–223

NUCLEAR
PHYSICS A

Double- β decay of ^{82}Se

R. Arnold^k, C. Augierⁱ, J. Baker^e, A. Barabash^h, D. Blumⁱ,
V. Brudanin^c, A.J. Caffrey^e, J.E. Campagneⁱ, E. Caurier^k, D. Dassié^a,
V. Egorov^c, R. Eschbach^a, T. Filipova^c, R. Gurriaran^a, J.L. Guyonnet^k,
F. Hubert^a, Ph. Hubert^a, S. Jullianⁱ, I. Kisel^c, O. Kochetov^c,
V.N. Kornoukhov^h, V. Kovalenko^c, D. Lalanneⁱ, F. Laplanche^{i,1},
F. Leccia^a, I. Linck^k, C. Longuemare^b, Ch. Marquet^a, F. Mauger^b,
P. Menrath^{a,2}, H.W. Nicholson^j, I. Pilugin^h, F. Piquemal^a, O. Purto^g,
J-L. Reyss^d, X. Sarazinⁱ, F. Scheibling^k, J. Suhonen^f, C.S. Sutton^j,
G. Szklarzⁱ, V. Timkin^c, R. Torres^a, V.I. Tretyak^g, V. Umatov^h,
I. Vanyushin^h, A. Vaille^a, Yu. Vasilyev^g, Ts. Vylov^c, V. Zerkov^g

NEMO Collaboration

^a CENBG, IN2P3-CNRS et Université de Bordeaux, 33170 Gradignan, France

^b LPC, IN2P3-CNRS et Université de Caen, 14032 Caen, France

^c JINR, 141980 Dubna, Russia

^d CFR, CNRS, 91190 Gif sur Yvette, France

^e INEL, Idaho Falls, ID 83415, USA

^f JYVÄSKYLÄ University, 40351 Jyväskylä, Finland

^g INR, 252028 Kiev, Ukraine

^h ITEP, 117259 Moscow, Russia

ⁱ LAL, IN2P3-CNRS et Université Paris-Sud, 91405 Orsay, France

^j MHC, South Hadley, MA 01075, USA

^k IReS, IN2P3-CNRS et Université Louis Pasteur, 67037 Strasbourg, France

Received 17 November 1997; revised 2 April 1998; accepted 15 April 1998

Abstract

The NEMO-2 tracking detector located in the Fréjus Underground Laboratory was designed as a prototype of the NEMO-3 detector to study neutrinoless (0ν) and two neutrino (2ν) double-beta decay ($\beta\beta$) physics. After 10 357 h of running with an isotopically enriched selenium source (2.17 mol yr of ^{82}Se) a $\beta\beta 2\nu$ decay half-life of $T_{1/2} = (0.83 \pm 0.10(\text{stat}) \pm 0.07(\text{syst})) \times 10^{20}$ yr was measured. Limits with a 90% C.L. on the ^{82}Se half-lives of 9.5×10^{21} yr for $\beta\beta 0\nu$ decay to the ground state, 2.8×10^{21} yr to the (2^+) excited state and 2.4×10^{21} yr for $\beta\beta 0\nu \chi^0$ decay with a Majoron (χ^0) were also obtained. © 1998 Elsevier Science B.V.

PACS: 23.40.-s; 14.60.Pq

Keywords: RADIOACTIVITY $^{82}\text{Se}(2\beta)$; measured 2ν associated 2β decay $T_{1/2}$, 0ν associated 2β decay $T_{1/2}$ lower limits.

1. Introduction

Two prototype detectors, NEMO-1 [1] and NEMO-2 [2] were constructed in a research and development program to study the feasibility of a much larger double beta decay experiment, NEMO-3. The NEMO-2 detector, designed for $\beta\beta$ background studies and $\beta\beta 2\nu$ decay, operated in the Fréjus Underground Laboratory (4800 w.m.e.). From 1992 to 1995 the $\beta\beta 2\nu$ decays of ^{100}Mo [3] and ^{116}Cd [4] were detected through measurements of the summed energy spectra, angular distributions and single electron spectra. Enriched and natural sources of selenium were installed in the NEMO-2 detector in the autumn of 1995 together with zirconium sources which are not reported on here. The zirconium data analysis, which is in progress, is rather difficult because of the radioactive pollution in the enriched source. Presented here are the results of measurements (10357 h) with ^{82}Se , which is one of the most favourable nuclides ($Q_{\beta\beta} = 2995$ keV) in the search for $\beta\beta 0\nu$ decay processes. The NEMO Collaboration has started to build the tracking detector NEMO-3 [5] which will be capable of studying $\beta\beta 0\nu$ decays of ^{100}Mo and other nuclei up to half-lives of $\sim 10^{25}$ yr, which corresponds to a Majorana neutrino mass of ~ 0.1 eV. The sensitivity to $\beta\beta 0\nu \chi^0$ and $\beta\beta 2\nu$ decays will be of $\sim 10^{23}$ yr and $\sim 10^{22}$ yr, respectively.

2. NEMO-2 detector

The NEMO-2 detector (Fig. 1) consists of a 1 m^3 tracking volume filled with helium gas and 4% ethyl alcohol. Vertically bisecting the detector is the plane of the source foil ($1 \text{ m} \times 1 \text{ m}$). Tracking is accomplished with long open Geiger cells with an octagonal cross section defined by $100 \mu\text{m}$ nickel wires. On each side of the source foil there are 10 planes of 32 cells which alternate between vertical and horizontal orientations. Collectively the cells provide three-dimensional tracking of charged particles.

A calorimeter made of scintillators covers two vertical opposing sides of the tracking volume. It consists of two planes of 25 scintillators ($19 \text{ cm} \times 19 \text{ cm} \times 10 \text{ cm}$) combined with low radioactivity photomultiplier tubes (PMT). The tracking volume and scintillators are surrounded with a lead (5 cm) and iron (20 cm) shield.

¹ Corresponding author. E-mail laplanch@lal.in2p3.fr; fax 33 169079404.

² Deceased.

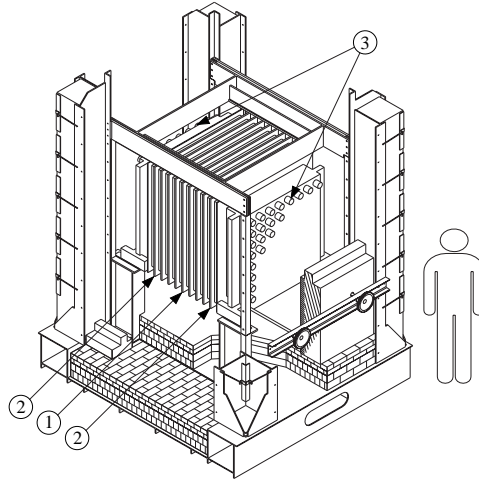


Fig. 1. The NEMO-2 detector without shielding. (1) Central frame with the source plane capable of supporting plural source foils. (2) Tracking device of 10 frames, each consisting of two perpendicular planes of 32 Geiger cells. (3) Two scintillator arrays each consisting of 5 by 5 counters. In the earlier experiment with molybdenum sources the scintillator arrays were 8 by 8 counters as depicted here.

2.1. Selenium sources

The source plane is divided into two halves. The first is a 156.6 g isotopically enriched selenium foil (97.02% is ^{82}Se). The second half is a 133.7 g foil of natural selenium of which 8.73% is ^{82}Se . The sources are composed of strips which were produced using a special technique to deposit selenium powder on thin films. The thickness of the foils is $\sim 50 \text{ mg/cm}^2$ for the enriched and $\sim 43 \text{ mg/cm}^2$ for the natural one. Radioactive impurities in both foils were measured with HPGe detectors in the Fréjus Underground Laboratory before installation in the NEMO-2 detector. The upper limits (90% C.L.) on the measured contaminations obtained in the enriched and natural selenium foils for the four isotopes ^{214}Bi , ^{208}Tl , ^{228}Ac and ^{234m}Pa are given in Table 1. Some activities from ^{40}K were found in both foils and are also included in Table 1.

Limits on the different levels of contamination between the foils were also obtained with the NEMO-2 detector by analyzing electron events involving γ rays, as explained in the section devoted to backgrounds. Two “hot” spots were found in the enriched selenium

Table 1

Upper limits (90% C.L.) and values on measured contaminations of the enriched and natural selenium foils. For each isotope the results obtained with HPGe detectors are given in mBq/kg

	^{214}Bi	^{208}Tl	^{228}Ac	^{234m}Pa	^{40}K
Enriched Se	<4.2	<2.5	<4	<33	200 ± 30
Natural Se	<5	<2	<5	<16	117 ± 16

foil and four “hot” spots in the natural foil. These regions of high activity were most likely introduced during the installation of the sources and their characteristics are given in the section on backgrounds.

2.2. Performances

Details of the performances and parameters are described elsewhere [2] while the most salient characteristics are briefly outlined here. Three-dimensional measurements of charged particle tracks are provided by the array of Geiger cells. The transverse position is given by the drift time and the longitudinal position by the plasma propagation times. The transverse resolution is $500\ \mu\text{m}$ and the longitudinal resolution is 4.7 mm. Track reconstruction is accomplished with a pattern recognition program based on a cellular automaton and an elastic neural network [6]. A tracking method based on the Kalman filter [7] was previously used in the $\beta\beta$ decay analysis with NEMO-2. Though similar results are obtained with both methods, the speed of the track reconstruction is greater and a gain of efficiency of $\sim 9\%$ is obtained with the present method.

The calorimeter energy resolution (FWHM) is 18% at 1 MeV with a time resolution of 275 ps (550 ps at 0.2 MeV). A laser and fiber optics device is used to check the stability of the scintillation detectors.

A trigger requiring two scintillation counters and four Geiger frames normally runs at a rate of 0.01–0.04 Hz depending on the radon levels in the laboratory. This trigger rate is too low for an efficient survey of the experiment, so a second trigger requiring only one counter with an energy greater than 1.3 MeV was added.

2.3. Event definition

An electron is defined by a track linking the source foil and one scintillator. The maximum scattering angle along the track has to be less than 20° to reject hard scattering situations. A photon is recognized as one or two adjacent fired scintillators without an associated particle track. For photons and electrons an energy deposited greater than 200 keV is required in order to obtain sufficiently good time resolution. The two-electron events are defined by two tracks which have a common vertex and are associated with two fired scintillators with a deposited energy of at least 200 keV in each one. A cut on the angle between the two electron tracks, $\cos \alpha \leq 0.6$, is applied as explained in the section devoted to the results. In the analysis a two-electron event is identified as $(2e)$ and electron–photon event as $(e\gamma)$.

In the coordinate system of the detector (Fig. 2) the origin of the axes is at the center of the source plane with the x -axis being horizontal and the y -axis vertical. Both foils are symmetrical with respect to the y -axis. The enriched selenium foil has positive x coordinates. The “hot” zones are represented by circles on the figure.

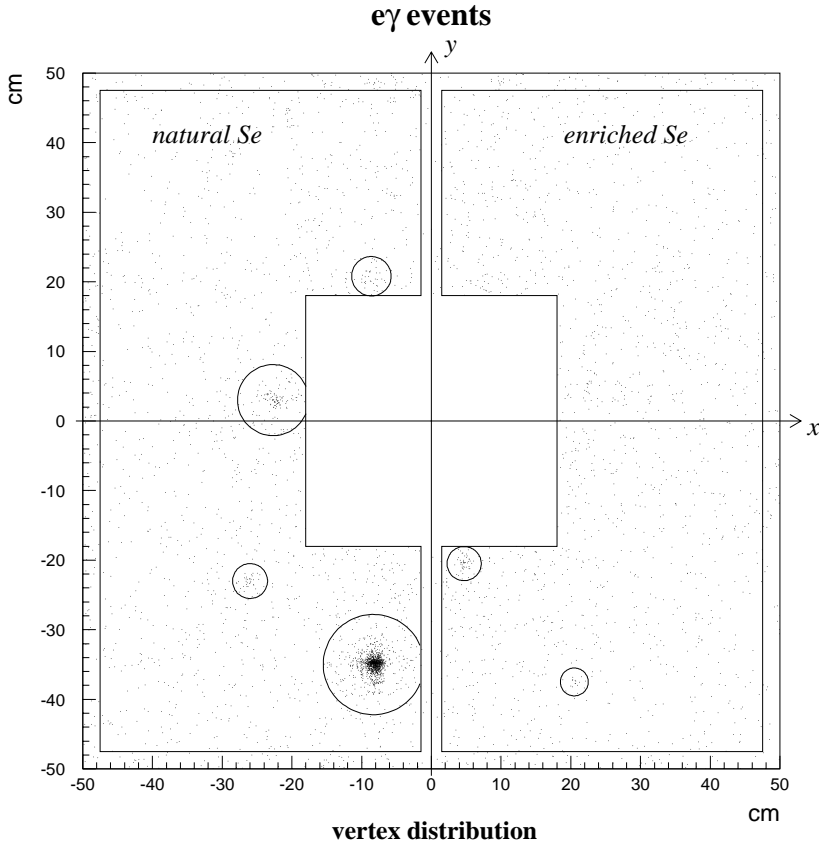


Fig. 2. The vertex position of $e\gamma$ events in the natural and enriched sources is displayed in the figure. The “hot” zones inside the circles are removed in the analysis. In the center of the source plane, zirconium sources were installed but are not considered here.

3. Backgrounds

The “external” background is due to photons originating from outside of the tracking detector and interacting with the source foils or with the scintillators. Compton electrons produced in the scintillators and crossing the tracking device are rejected by time-of-flight analysis. Compton electrons produced in the source foils can generate a secondary electron by the Möller effect. A double Compton effect or pair production can also occur. These $2e$ background events cannot be rejected by time-of-flight cuts. The dominant contribution to the external background comes from the flux of photons emitted by radon located between the tracking detector and the shielding. Another source of background is due to the flux of photons emitted by the PMTs.

Radioactive pollution in the source foils produces a background identified as “internal”. An electron which gives rise to the Möller effect, or is associated with an internal conversion electron, or a Compton electron can produce $2e$ background events.

To study the nature of the background in the source foils $e\gamma$ events were examined.

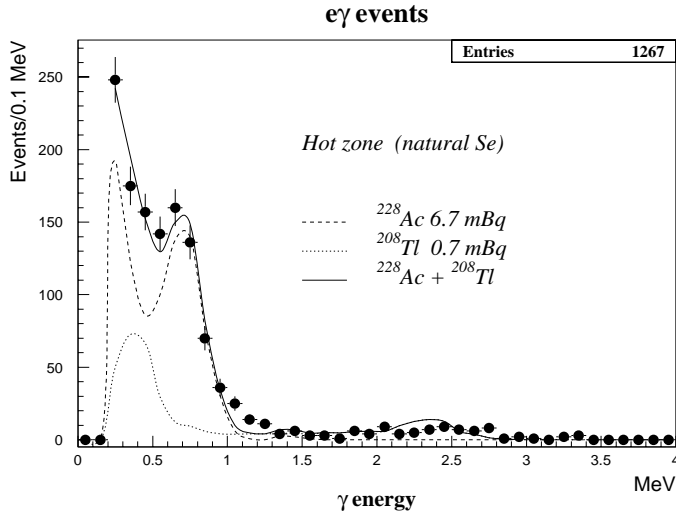


Fig. 3. The photon energy spectrum of the most active zone in the natural selenium foil is characterized here by two components with very high levels of pollution. The simulation reproduces very well the experimental data.

Only $e\gamma$ “back-to-back” events (both scintillator arrays fired) were selected in this analysis because time-of-flight criteria cannot distinguish between the Compton effect originating in the scintillators and in the foils when the electron and photon are detected in the same scintillator array. The hypothesis that the same photon flux crosses the enriched and natural selenium foils was checked at the 5% level by a set of $e\gamma$ events with a Compton electron generated in the scintillators and selected by time-of-flight analysis.

Before analyzing the backgrounds the hot zones were located and characterized. Locations were found with the vertex distribution and to exclude events due to poor vertex reconstruction the surrounding neighborhoods were cut from the data sample. Information about the nature of the pollution was extracted from the photon energy spectrum. The spectrum for the most active zone in the natural selenium is shown in Fig. 3. The spectrum shape is explained with two components, ^{228}Ac and ^{208}Tl . Proportionally these zones have a very high level of activity with respect to the non-polluted areas. The hot zones which were removed from the analysis correspond to 7.6% of the natural selenium foil and 0.8% of the enriched selenium foil.

From the experimental record of $e\gamma$ events in the enriched selenium (1403) and natural selenium (1243) one derives the counting ratio between the two foils, 1.13 ± 0.07 (the error includes the uncertainty in the left–right symmetry of the external photon flux). A 1.22 calculated ratio between the foils is obtained by taking into account the difference in the foil masses, the composition of the foils and the removed polluted zones. This value is compatible with the experimental result. A fit of the γ energy spectrum from the natural selenium foil was made using the spectrum from the enriched foil (renormalized by the factor 1.22) and taken as free parameters were the

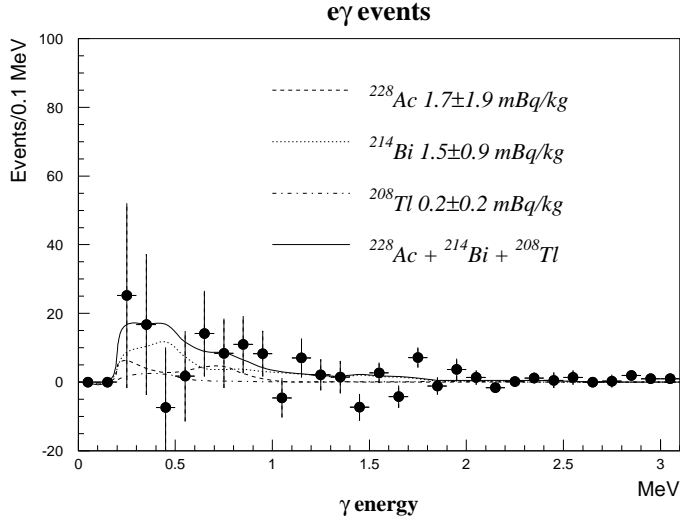


Fig. 4. This spectrum is the difference between natural and enriched foils spectra, normalized as explained in the section on backgrounds. The contributions due to ^{228}Ac , ^{214}Bi and ^{208}Tl , which are small and compatible with zero, are used to estimate the systematics due to background subtraction.

spectra of ^{228}Ac , ^{214}Bi and ^{208}Tl . The result is shown in Fig. 4 where the difference between the two experimental spectra is plotted, the small contaminations extracted from the fit are compatible with zero and are used to estimate the systematic uncertainties in the background subtraction. All the Monte Carlo simulations were made with the GEANT 3.21 program.

4. Results

4.1. $\beta\beta 2\nu$ signal

In the first step the 2e events are selected by time-of-flight analysis. For each event the probability of it being an internal (P_{int}) or an external (P_{ext}) source event is computed. By applying the cuts $P_{\text{int}} > 10^{-2}$ and $P_{\text{ext}} < 10^{-5}$ very few background events are expected in each foil. Given these cuts the vertex distribution (Fig. 5) in the source plane shows a clear excess of 2e events in the enriched selenium (positive x -positions). The raw data energy spectra in the enriched selenium (234 events) and natural selenium (74 events) are shown in Fig. 6. In the energy range 0.45 to 2.4 MeV, which is of interest in $\beta\beta 2\nu$, the number of events in each foil are 231 and 73, respectively.

The 2e background in the enriched foil is calculated by using 2e events in the natural foil and the measured contaminations from the detector itself and from a Ge detector.

In natural selenium 8.4 ± 1.2 2e events are induced by the ^{40}K activity (117 ± 16 mBq/kg) as measured with the Ge detector. A contribution of 12.0 ± 1.8 2e events from $\beta\beta 2\nu$ decay is calculated for the ^{82}Se component in the natural selenium foil

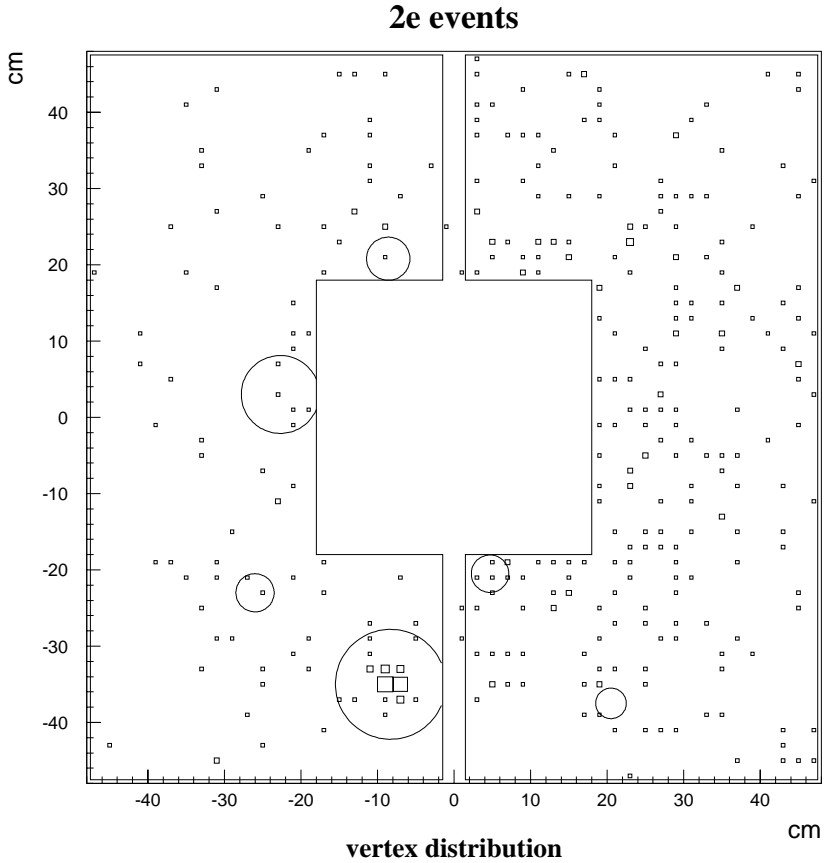


Fig. 5. The vertex distribution shows a clear excess of 2e events in the enriched selenium foil. The events located in the “hot” zones found in the *ey* analysis have been removed.

assuming $T_{1/2}^{2\nu} = 0.83 \times 10^{20}$ yr.

Next uncertainties due to the difference of contamination between the two sources are calculated. The ^{228}Ac , ^{214}Bi and ^{208}Tl activities deduced from the *ey* event analysis (Fig. 4) give uncertainties in the 2e background subtraction of 2.5, 4, and 1.5 events, respectively. The analysis of one-electron events yields a limit of seven 2e events in the difference of ^{234m}Pa contamination (<6 mBq/kg) between the two sources.

From the external background of $52.6 \pm 8.5(\text{stat}) \pm 2.2(\text{syst})$ events in the natural foil, $64.2 \pm 10.4(\text{stat}) \pm 5.4(\text{syst})$ background events are computed in the enriched foil by applying the normalization factor 1.22 ± 0.09 . The normalization factor used in the case of the *ey* analysis is applicable because the increase of the Möller effect is roughly canceled by the rejection of electrons due to the increase of their energy loss. A 5% error in the normalization factor because of this approximation is added to the uncertainty (5%) due to the photon flux hypothesis as explained in Section 3.

The distributions of the angle (α) between the two emitted electrons in enriched selenium with backgrounds subtracted (Fig. 7b) and in natural selenium (Fig. 7a) are

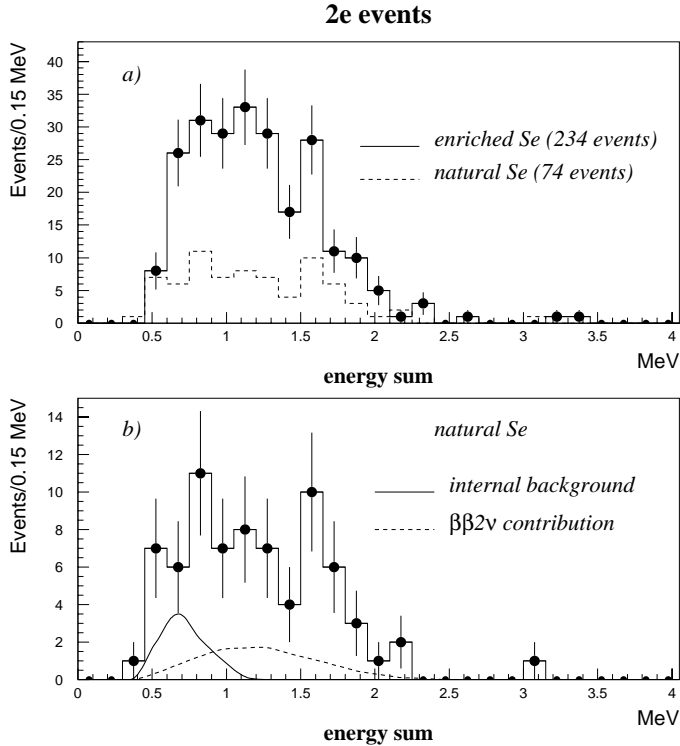


Fig. 6. (a) The experimental distributions of the 2e energy sum in enriched and natural selenium foils are shown. (b) In natural selenium the internal background contribution (8.4 events) is calculated from Ge measurements of ^{40}K . A $\beta\beta$ contribution of twelve events is computed. About two thirds of the experimental 2e events are due to external background (52.6 events).

very different. In the natural selenium, the angular distribution is peaked in the forward direction, as expected from the external background. After background subtraction the $\cos \alpha$ distribution in the enriched selenium was compared to a simulation of a pure $\beta\beta 2\nu$ decay spectrum. In order to improve the signal-to-background ratio the cut, $\cos \alpha \leq 0.6$, was applied in the selection of 2e events. With all the cuts applied to the 2e events an overall Monte Carlo $\beta\beta 2\nu$ efficiency of $[1.39 \pm 0.05]\%$ is computed (the uncertainty in the Monte Carlo calculation is estimated to 3.7%).

The energy distribution of a single electron in the two-electron events is also different for $\beta\beta 2\nu$ and background. These distributions are shown in Fig. 8, here the simulated energy spectrum reproduces the experimental spectrum in the enriched selenium foil. From this distribution an uncertainty of 3 events due to the energy calibration error (10 keV for 200 keV electrons) is computed.

The $\beta\beta 2\nu$ energy spectrum in the enriched selenium ($149.1 \pm 18.4(\text{stat}) \pm 12.6(\text{syst})$ events) is obtained by subtracting from the raw data spectrum ($231 \pm 15.2(\text{stat})$ events) the background spectrum ($81.9 \pm 10.4(\text{stat}) \pm 6.0(\text{syst})$ events, $17.7 \pm 2.7(\text{syst})$ from ^{40}K and $64.2 \pm 5.4(\text{syst})$ from external background). This spectrum is fitted (Fig. 9) to the simulated spectrum and one gets,

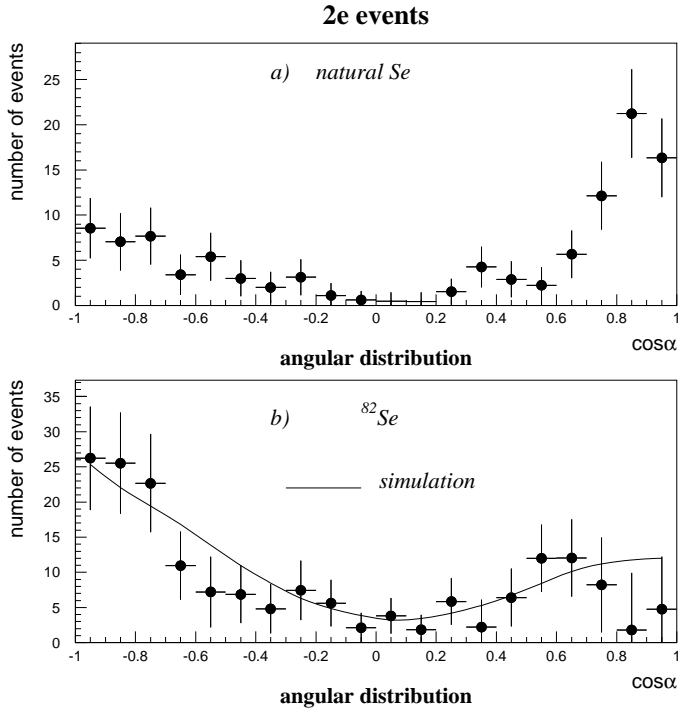


Fig. 7. (a) The angular distribution (α is the angle between the two electron tracks) is peaked in the forward direction in the natural selenium foil (internal background and $\beta\beta 2\nu$ contribution subtracted). (b) In the enriched selenium foil the simulation is in agreement with the experimental spectrum (background subtracted).

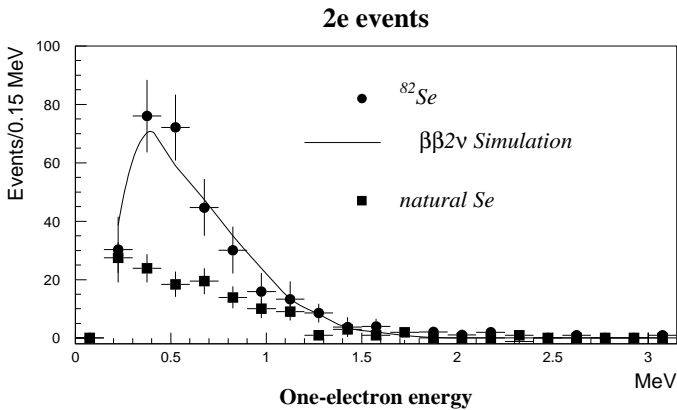


Fig. 8. The single electron energy spectrum in natural selenium (internal background and $\beta\beta 2\nu$ contribution subtracted) has a different shape from the energy spectrum in enriched selenium (internal and external background subtracted). The simulation agrees with the experimental data.

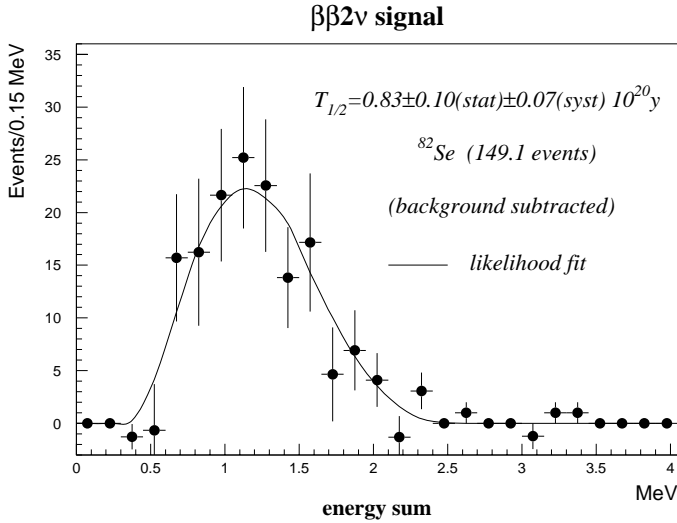


Fig. 9. The $\beta\beta 2\nu$ half-life $T_{1/2}$ has been obtained by the fit of the $2e$ energy spectrum in enriched selenium (background subtracted) with the $\beta\beta 2\nu$ simulated spectrum using the likelihood method.

Table 2

Systematic errors. All the errors which contribute to the signal are listed here in number of events

Source of the systematics	Number of events
Monte Carlo	5.5
Tracking	3.0
Energy calibration	3.0
^{40}K (enriched foil)	2.7
External background	5.4
^{228}Ac , ^{214}Bi , ^{208}Tl	4.9
^{237m}Pa	7.0
Total systematic error	12.6

$$T_{1/2}^{2\nu} = [0.83 \pm 0.10(\text{stat}) \pm 0.07(\text{syst})] \times 10^{20} \text{ yr.}$$

The final systematic error includes an uncertainty in the track reconstruction and the uncertainties due to the difference of contamination between the foils. In Table 2 are summarized all the systematics.

4.2. Limits on 0ν modes

Monte Carlo simulations of the summed electron energy spectrum are shown in Fig. 10 for $\beta\beta 0\nu$ decays to the ground states, with and without Majoron emissions, and for decays to the excited 2^+ state (776 keV).

Half-life limits extracted from the data are given in Table 3. The energy windows, number of events, backgrounds, and efficiencies are also given. Limits are computed with the formula for Poisson processes with background [10].

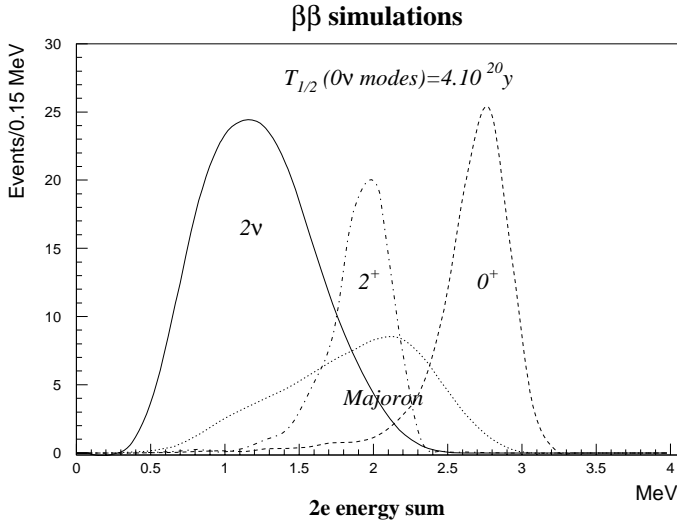


Fig. 10. The Monte Carlo $\beta\beta 0\nu$ spectra plotted for half-lives of 4×10^{20} yr show the detector responses and explain the ranges selected in Table 3 to compute the half-life limits.

Table 3

Half-life limits. For each decay channel an energy window is defined, the corresponding number of experimental events, the number of calculated background $+\beta\beta 2\nu$ events, the calculated upper limit (90% C.L.) of the number of events, the efficiency, and the half-life limit (90% C.L.) are given. Half-life limits at 68% C.L. from this experiment and from the TPC experiment [8,9] (68% C.L.) are also included for comparison

Channel	$0^+_{\text{g.s.}}$	Majoron	2^+
Window (MeV)	[2.4, 3.15]	[2.1, 3.]	[1.8, 2.25]
Number of events	1	5	16
Background $+\beta\beta 2\nu$	1.2	5.0	19.4
Upper limit (events)	<3.2	<5.1	<6.5
Efficiency (%)	3.45	1.4	2.05
$T_{1/2}(10^{21}$ yr) (90%)	>9.5	>2.4	>2.8
$T_{1/2}(10^{21}$ yr) (68%)	>17	>4.4	>4.5
$T_{1/2}(10^{21}$ yr) (68%) [8,9]	>27	>1.6	>3.4

5. Discussion

The $\beta\beta 2\nu$ half-life value which is obtained here can be compared with previous geochemical experimental results: $(1.30 \pm 0.05) \times 10^{20}$ yr [11] (this is an average value for seventeen independent measurements which were done up to 1986) and with a more recent result $(1.2 \pm 0.1) \times 10^{20}$ yr [12].

In an earlier direct detection experiment which used a TPC [9] 89.6 $\beta\beta 2\nu$ events were detected in ^{82}Se and a half-life value $(1.08^{+0.26}_{-0.06}) \times 10^{20}$ yr was obtained. In 1991 Manuel [13] analysed all existing ^{82}Se results and proposed 1×10^{20} yr for the half-life.

The result produced here is 1.2–1.6 times lower than in previous experiments. But taking into account possible systematic errors in both geochemical ($\sim 30\%$ as mentioned

in Ref. [12]) and direct (not explicitly mentioned in Ref. [9]) experiments, one can conclude that there is no serious discrepancy between present and previous values. Consequently the NEMO Collaboration is confident that the most precise value for the ^{82}Se half-life has been obtained in the NEMO-2 experiment presented here.

It is interesting to note that the ^{82}Se half-life value produced in the present paper confirms (in an indirect way) the conclusion of Manuel [13,14] that ^{130}Te and ^{128}Te half-life values are respectively $\sim 0.8 \times 10^{21}$ yr and $\sim 2 \times 10^{24}$ yr. In geochemical experiments with minerals which contain Se and Te, the ratio of $T_{1/2}(^{82}\text{Se})/T_{1/2}(^{130}\text{Te})$ has had the following values: 7.3 ± 0.9 [15], 12.5 ± 0.9 [11] and 10 ± 2 [16]. The gas retention age problem has no effect on the half-life ratio. Taking into account the ^{82}Se half-life value from the NEMO-2 experiment, one can conclude that the ^{130}Te half-life cannot be higher than 1.3×10^{21} yr and the most probable value is close to $\sim 0.8 \times 10^{21}$ yr. The $^{128}\text{Te}/^{130}\text{Te}$ half-life ratio is known with high accuracy (see Refs. [13,17]), thus the most probable value of the ^{128}Te half-life is $\sim 2 \times 10^{24}$ yr. These values (0.8×10^{21} yr and 2×10^{24} yr) are in agreement with those from Refs. [12–14,18,19], but in strong disagreement with results of T.Kirsten et al. ($(1.5–2.75) \times 10^{21}$ yr and $> 5 \times 10^{24}$ yr) [11] and Bernatowicz et al. ($(2.7 \pm 0.1) \times 10^{21}$ yr and $(7.7 \pm 0.4) \times 10^{24}$ yr) [17]. To finally solve this problem a direct observation of $\beta\beta 2\nu$ decay of ^{130}Te is needed which will in turn yield a precise value of the ^{128}Te half-life. It is important to know this value as it is used to obtain a strong limit on the Majorana neutrino mass ($\langle m_\nu \rangle$), Majoron to Majorana neutrino coupling constant (g_M) and other theoretical parameters (see, Refs. [17,20,21] and below).

Using the $\beta\beta 2\nu$ half-life value presented here and the phase-space factor $G = 4.3 \times 10^{-18} \text{ yr}^{-1}$ (for the bare axial-vector coupling constant $g_A = 1.254$ [22]), one obtains the nuclear matrix element (NME) $M_{2\nu} = 0.053_{-0.004}^{+0.006}$ (scaled by the electron rest mass) or $M_{2\nu} = 0.104_{-0.009}^{+0.012} \text{ MeV}^{-1}$. If one wants to use the effective value of the axial-vector coupling constant, $g_A = 1.0$, one ends up with the phase-space factor (G scales as g_A^4) $G = 1.7 \times 10^{-18} \text{ yr}^{-1}$ and the respective nuclear matrix element values $M_{2\nu} = 0.083_{-0.007}^{+0.009}$ or $M_{2\nu} = 0.163_{-0.014}^{+0.018} \text{ MeV}^{-1}$. These values are in good agreement with the shell-model calculations [23] $M_{2\nu} = (0.16–0.21) \text{ MeV}^{-1}$ and can be explained well in the framework of the multiple-commutator model (MCM) [24], where the matrix element value $M_{2\nu} = (0.072–0.14) \text{ MeV}^{-1}$ was obtained. This was derived by first studying the beta feeding of the involved mother and daughter nuclei of double beta decay and thus fixing the effective hamiltonian by single beta decay leaving the double beta decay rates to the ground state and excited states as genuine predictions of the model. It has to be noted that the above procedure is not used much in the random-phase approximation (RPA) type theories where the two-neutrino double beta decay rate to the ground state is used to fix the parameters of the effective hamiltonian [25,26].

In Table 3 besides the limits presented here on 0ν decay modes of ^{82}Se the limits obtained by Moe et al. with a TPC are presented. The results of both experiments are compatible.

Using the $\beta\beta 0\nu$ half-life limit deduced here and the NMEs from Refs. [23,27–30] one finds a lower limit for the effective Majorana neutrino mass $\langle m_\nu \rangle < (8–16) \text{ eV}$.

The best limit, $\langle m_\nu \rangle < (0.6–1.6)$ eV is obtained from a germanium experiment [31] using the five above referenced NMEs.

A limit on the Majoron-Majorana neutrino coupling constant for “ordinary” singlet Majoron [32–34] is derived from the result presented here by the already referenced NMEs [23,27–30] and the phase-space factor $4.84 \times 10^{-16} \text{ yr}^{-1}$ [22] yielding $g_M < (2.3–4.3) \times 10^{-4}$. The best present limit can be obtained from geochemical experiments with ^{128}Te . Using the half-life value $T_{1/2} = 2 \times 10^{24} \text{ yr}$, discussion above, as a limit for decay with the emission of a Majoron, the phase space integral $G = 4.43 \times 10^{-18} \text{ yr}^{-1}$ [22] and the NMEs from Refs. [27–30,35], one obtains $g_M < (0.7–1.4) \times 10^{-4}$ (the limit 1.4×10^{-4} is obtained with recent shell model calculations of a NME [35]). Limits close to the one derived here are given by the ELEGANT V experiment with a ^{100}Mo source ($g_M < 7.3 \times 10^{-5}$ at 68% C.L.) [36], by a ^{136}Xe experiment ($g_M < 2.4 \times 10^{-4}$ at 90% C.L.) [37] and by NEMO-2 with a ^{116}Cd source ($g_M < 1.2 \times 10^{-4}$ at 90% C.L.) [4].

6. Conclusion

The selenium data together with the zirconium data are the last experiments to be carried out with the NEMO-2 detector which is now dismantled. The natural selenium sources were slightly polluted during installation but reliable results have been extracted. In summary the NEMO-2 detector has been highly effective at a number of double beta decay measurements and as a prototype it has provided invaluable experience for the successful operation of NEMO-3. The mounting of NEMO-3 in the Fréjus Underground Laboratory will start in 1998 and data collection is foreseen to begin about one year later.

Acknowledgements

The authors would like to thank the Fréjus Underground Laboratory staff for their technical assistance in running the experiment.

The portions of this work conducted in Russia were supported by RFFI grant number 97-02-17344.

References

- [1] D. Dassié et al., Nucl. Instr. and Meth. A 309 (1991) 465.
- [2] R. Arnold et al., Nucl. Instr. and Meth. A 354 (1995) 338.
- [3] D. Dassié et al., Phys. Rev. D 51 (1995) 2090.
- [4] R. Arnold et al., Z. Phys. C 72 (1996) 239.
- [5] NEMO-3 Proposal, LAL preprint 94-29 (1994).
- [6] I. Kisel et al., Nucl. Instr. and Meth. A 387 (1997) 433.
- [7] P. Billoir, Nucl. Instr. and Meth. A 255 (1984) 352.

- [8] M.K. Moe, S.R. Elliott and A.A. Hahn, Proc. VIIIth Moriond Workshop 5th Force – Neutrino Physics, Les Arcs, Savoie, January 23–30, 1988, ed. O. Fackler and J. Tran Thanh Van (Editions Frontières, 1988) p. 47.
- [9] S.R. Elliot et al., Phys. Rev. C 46 (1992) 1535.
- [10] O. Helene, Nucl. Instr. and Meth. B 212 (1983) 319;
Particle Data Group, Phys. Rev. D 50 (1994) 1281.
- [11] T. Kirsten et al., Proc. Nuclear Beta Decay and Neutrino, Osaka, 1986, ed. T. Kotani et al. (World Scientific, Singapore) p. 81.
- [12] W.J. Lin et al., Nucl. Phys. A 481 (1988) 477.
- [13] O.K. Manuel, J. Phys. G 17 (Supplement) (1991) 221.
- [14] O.K. Manuel, Proc. Nuclear Beta Decay and Neutrino, Osaka, 1986, ed. T. Kotani et al. (World Scientific, Singapore) p. 71.
- [15] W.J. Lin et al., Nucl. Phys. A 457 (1986) 285.
- [16] B. Srinivasan et al., Econ. Geol. 68 (1973) 252.
- [17] T. Bernatowicz et al., Phys. Rev. C 47 (1993) 806.
- [18] N. Takaoka and K. Ogata, Z. Naturforsch. 21a (1966) 84.
- [19] N. Takaoka, Y. Motomura and K. Nagao, Phys. Rev. C 53 (1996) 1557.
- [20] J. Suhonen and O. Civitarese, J. Phys. G 20 (1994) 347.
- [21] K. Zuber, Phys. Rev. D 56 (1997) 1816.
- [22] J. Suhonen and O. Civitarese, Phys. Rep. (1998), in press.
- [23] E. Caurier et al., Phys. Rev. Lett. 77 (1996) 1954.
- [24] M. Aunola and J. Suhonen, Nucl. Phys. A 602 (1996) 133.
- [25] S. Stoica, Phys. Rev. C 49 (1994) 2240.
- [26] J. Toivanen and J. Suhonen, Phys. Rev. C 55 (1997) 2314.
- [27] K. Muto, E. Bender and H.V. Klapdor, Z. Phys. A 334 (1989) 187.
- [28] T. Tomoda, Rep. Prog. Phys. 54 (1991) 53.
- [29] J. Suhonen, S.B. Khadkikar and A. Faessler, Nucl. Phys. A 535 (1991) 509.
- [30] J. Engel, P. Vogel and M.R. Zirnbauer, Phys. Rev. C 37 (1988) 73.
- [31] M. Gunther et al., Phys. Rev. D 55 (1997) 54.
- [32] Y. Chikashige, R.N. Mohapatra and R.D. Peccei, Phys. Lett. B 98 (1981) 265.
- [33] Z.G. Berezhiani, A.Yu. Smirnov and J.W.F. Valle, Phys. Lett. B 291 (1992) 99.
- [34] C.P. Burgess and J.M. Cline, Phys. Lett. B 298 (1993) 141.
- [35] E. Caurier et al., in Proc. Workshop on Calculation of double beta decay matrix elements, Prague, 27–31 May, 1997, to be published.
- [36] H. Ejiri et al., Nucl. Phys. A 611 (1996) 85.
- [37] J.-C. Vuilleumier et al., Phys. Rev. D 48 (1993) 1009.